Improvement the post-processing quality in lock-in thermography

Anna V. Stoynova and Borislav B. Bonev

***Abstract*—**Active thermography is widely used method for non-destructive testing. In contrast to passive thermography, in active thermography using of raw data post-processing is necessary in all cases, especially in lock-in thermography. In lock-in thermography, defects cause thermal wave phase difference between defect and sound area. Aim of the post-processing is to calculate phases correctly for each pixel from raw thermogram sequence. Typically, the processing is performed on a part of the thermogram sequence and the question arises as to how to select this part. Depending on the used part of the thermogram sequence for the post-processing, the searched defects in some cases cannot be detected despite the sufficient phase difference between the defect and sound area for their detection is present. The aim of this study is to investigate the impact of this and other factors on the quality of the post-processing (evaluated with phasegram quality) and to define an algorithm for improving the quality of the post-processing. Modelling and real thermographic measurements were used to investigate this influence. The results from modelling and from real lock-in thermography measurements shows that by using of the proposed methods can be avoided decreasing of defects detectability caused by post-processing. It is proposed algorithm including proposed methods for contrast increasing. The problems associated with phasegram sharpness and phasegram pixel saturation are presented.

***Keywords*—** lock-in thermography, phasegram, phase contrast, post-processing.

I. Introduction

At present, a strong interest exists towards the use of active thermography methods in non-destructive material and structural analyses [1], [2]. A forced thermal excitation is used in active thermography in contrast to passive thermography. Different kind of excitation sources (optical, electromagnetic, ultrasound etc.) can be employed for intentional temperature change. There are different types of active thermography methods – short-pulse, long-pulse, lock-in [2]. The lock-in thermography requires post-processing techniques that is more complex, but it has significant advantages than other active thermography methods - is influenced to a lesser extent by environment reflections, noises, uneven heating, differences in emissivity [3], [4]. Due to these advantages, lock-in thermography is widely used method for hidden defects detection [5-8].

The heighten demand especially of lock-in thermography is associated with the both price reduction of the infrared cameras and the computing power increase of the used computer systems. This involves complicated post-processing of thermograms resulting in more accurate quantitative evaluations [9].

Optimization of pre-processing and post-processing in active thermography is actual research problem. In [4], an off-line methodology has been applied for optimization of lock-in frequencies choice in case of heat source modulation into a train of square waves. Complex lock-in analyses have been provided by two alternative low pass filtering methods in the time domain (averaging) and in the frequency domain (harmonics suppression).

In this paper, another off-line methodology is presented to enhance information from lock-in IR signals in case of optical heat source modulation into a train of sin waves. The quality of post-processing (evaluated with quality of phasegrams, the most used image for defects detection) in lock-in thermography is studied and analysed depending on post-processing method used. Improving the post-processing quality also allows improving the energy efficiency of the lock-in thermography measurement, as the same phasegram quality can be obtained with lower temperature change respectively lower excitation energy [10]. In addition, lower excitation energy from the excitator allows testing of objects, which can otherwise be destroyed from the excitation with high energy due to higher thermal stress.

The methodology based on modelling and measurements of temperature signals from infrared thermography is used. Some cases, in which the defects detection quality is significantly decreased, are presented and corresponded methods for correction in such cases are proposed. The proposed methods are merged into a common algorithm for post-processing in lock-in thermography in order to obtain maximum phasegrams quality.

II. Lock-in thermography processing methods

In lock-in thermography, periodically illumination to inject thermal waves into the specimen is used. The thermal response

The paper is published with the support of the project No. DN 17/16 of the National Science Fund of Bulgaria.

This is an extended version of the paper with title "Improvement the temperature signal filtering in lock-in thermography", presented in CSCC2018 conference.

A. V. Stoynova is with the Microelectronics Department, Technical University of Sofia, 1797 Sofia, Bulgaria (corresponding author to provide phone: +359-882-142522; e-mail: ava@ecad.tu-sofia.bg).

B. B. Bonev is with the Microelectronics Department, Technical University of Sofia, 1797 Sofia, Bulgaria (e-mail: bonev@ecad.tu-sofia.bg).

is recorded at the same time using infrared camera. The light intensity (when the excitator is halogen lamp) can be modulated with a sinusoidal waveform signal. The frequency of this signal is named lock-in frequency. The created thermal waves penetrate object's surface and it is partially reflected by its non-homogeneities. Due to interference of the reflected portions of the wave with the input thermal wave, phase shifts of the local surface temperature oscillating at the lock-in frequency can be derived. The surface temperature variations are captured via infrared camera in series of thermograms (thermogram sequence). The amplitude and the phase of the sinusoidal wave pattern at each thermogram sequence pixel after post-processing are computed. The resultant images are a phasegram and/or an ampligram.

Non-homogeneities of the object are better detected from the phasegrams than from the raw thermograms because phase images are less affected by surface emissivity variations, uneven heating and environment reflections. Nevertheless, to obtain the temperature change and phase difference, caused only by the excitation source, it is needed special post-processing [3], [4]. One of the methods for amplitude and phase calculation of each thermogram sequence pixel is digital lock-in correlation [3], [4]. In this method, two intermediate images are computed – in-phase image and quadrature image. These images are necessary for the subsequent calculation of the ampligram and phasegram. Each pixel of in-phase and quadrature images is obtained by [3]:

$$S^{0^\circ}(x,y) = \frac{1}{Nn}\sum_{k=1}^{N}\sum_{m=1}^{n} F_{k,m}(x,y) K_m^{0^\circ}, \quad (1)$$

$$S^{-90^\circ}(x,y) = \frac{1}{Nn}\sum_{k=1}^{N}\sum_{m=1}^{n} F_{k,m}(x,y) K_m^{-90^\circ}, \quad (2)$$

where $S^{0^\circ}(x,y)$ – value of in-phase image's pixel (x,y), $S^{90^\circ}(x,y)$ – value of quadrature image's pixel (x,y), x – row of thermogram, y – column of thermogram, N – number of lock-in periods for which the calculation is performed, n – number of captured thermograms per lock-in period, $F_{i,j}(x,y)$ – value of thermogram's pixel i from lock-in period j, K_{m0° - correlation coefficient for computation of the in-phase image, $K_m^{-90^\circ}$ - correlation coefficient for computation of the quadrature image.

The correlation coefficients are values of sinusoidal wave and they are calculated as follows [3]:

$$K_m^{0^\circ} = 2\sin\left(\frac{2\pi(m-1)}{n}\right), \quad (3)$$

$$K_m^{-90^\circ} = -2\cos\left(\frac{2\pi(m-1)}{n}\right), \quad (4)$$

Ampligram and phasegram are calculated as follows [3]:

$$S_A(x,y) = \sqrt{S^{0^\circ}(x,y)^2 + S^{-90^\circ}(x,y)^2}, \quad (5)$$

$$S_P(x,y) = \tan^{-1}\left(\frac{S^{-90^\circ}(x,y)}{S^{0^\circ}(x,y)}\right). \quad (6)$$

where $S_A(x,y)$ – value of the ampligram's pixel (x,y), $S_P(x,y)$ – value of the phasegram's pixel (x,y).

In our previous study [9] it is proposed adding of correction coefficients in the correlation function, which can change its frequency and initial phase. In result, equations (3) and (4) are transformed as follows:

$$K_m^{0^\circ} = 2\sin\left(\frac{2\pi(100+d)(m-1)}{100n} - 2\pi t_d f_l\right), \quad (7)$$

$$K_m^{-90^\circ} = -2\cos\left(\frac{2\pi(100+d)(m-1)}{100n} - 2\pi t_d f_l\right), \quad (8)$$

where t_d [s] – time shift of the correlation function, f_l [Hz]– lock-in frequency, d [%] – frequency deviation.

III. Modelling of Temperature Signal

The correct calculation of amplitude and phase value for each thermogram sequence pixel (i.e. temperature signal) depends on post-processing. Different disturbance components are superimposed on the temperature signal. Disturbances in this case are:

1) thermal excitation from another excitation source;
2) environment reflections;
3) uneven heating;
4) different emissivity of the object surface's different areas.

A big thermogram sequence is obtained after lock-in thermography measurement. Before starting of post-processing, some questions arise:

1) Should the whole sequence of thermograms be used or only part of it (window)?
2) How to choose the window length?
3) How to choose the first and last thermogram if only part of the sequence of thermograms?

1D modelling of temperature signals is used in order to study the dependence from these parameters. There is a significant phase difference between the temperature signals of a defective area and a sound area in successful lock-in thermography measurement. The model contains two signals between which there is a phase difference. Disturbing signals are superimposed on the useful signal in order to simulate the above-described disturbances.

The temperature change over time at a given point on the tested object (so called temperature signal) captured with infrared camera in real lock-in thermography measurement is shown in Fig. 1. This signal is constructed from values of corresponding pixel from all thermograms in sequence.

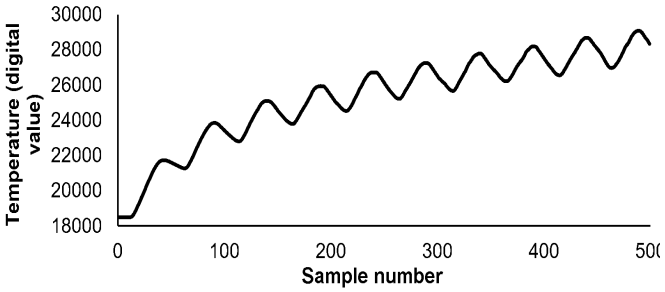

Fig. 1 temperature signal of a pixel from raw thermogram sequence

The approximation of the temperature signal is described mathematically with the following equations [10]:

$$F(k) = F_{mod}(k) + F_{noise}(k), \tag{9}$$

$$F_{mod}(k) = T_{initial} + ak + bk^2 + \Delta T sin\left(\frac{2\pi k}{n} + \psi_F\right), \tag{10}$$

$$F_{noise}(k) = \Delta T_{noise} \sin\left(\frac{2\pi k}{n_{noise}} + \psi_{noise}\right), \tag{11}$$

where $F(k)$ – model of the temperature signal, $F_{mod}(k)$ – a component of the model due to thermal modulation, $F_{noise}(k)$ – a noise component, $T_{initial}$ – initial temperature, a and b – coefficients, ΔT – an amplitude of temperature oscillation due to the modulation, k – number between 1 and n, n – number of samples per lock-in period, ψ_F – initial phase of the temperature oscillation, ΔT_{noise} – amplitude of temperature oscillation due to the noise, n_{noise} – number of samples in a noise period, ψ_{noise} – initial phase of the noise.

The impact of disturbing signals is simulated by the following parameters:

1) thermal excitation from another excitation source – with noise component $F_{noise}(k)$;
2) uneven heating – with different value of initial temperature $T_{initial}$ value for both signals;
3) different emissivity of different areas from object surface – also with initial temperature $T_{initial}$, because temperature signal value depends on emissivity of surface area.

The parameters values of the model are shown on Table I. The signal models are shown in graphical form in Fig. 2.

Parameter	Value at signal 1	Value at signal 2
$T_{initial}$ (°C)	25	30
a	0.2	0.2
b	-0.0002	-0.000195
ΔT (°C)	5	4.5
n	50	50
ψ_F (rad)	0.0628	0.0698
ΔT_{noise} (°C)	1	1
n_{noise}	5	8
ψ_{noise}	0.0209	0.1047

Table. I parameter values of the temperature signals model.

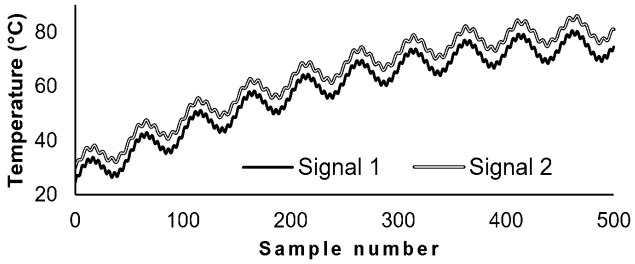

Fig. 2 temperature signal models in graphic form

IV. Post-processing of temperature signals model

The same method as for post-processing a sequence of thermograms obtained after a real thermogram measurement is used to determine the phase of both signals from the model. Equation (6) is used. The post-processing quality can be evaluated by phase contrast (12).

$$Phase\ contrast = \left| S_{P\,\text{signal}1} - S_{P_{\text{signal}2}} \right| \tag{12}$$

A. Time shift of the correlation function

Table II shows the phase contrast at different values of the correlation function's time shift - parameter t_d in (7) and (8).

Time shift (rad)	Phase contrast (rad)
0	0.02568011
-0.628	0.02568011
-1.709	3.115912544
-2.513	0.02568011

Table. II Phase contrast at different correlation function time shift

It can be seen that the correlation function time shift does not affect the phase contrast, except when saturation occurs (the first phase is approx. 1.57, and the second phase -1.57 or vice versa). In case of saturation, phase information is lost for the corresponding temperature signal. Therefore, in the case of saturation in phasegram, which affects the area of interest, can be used change of the correlation function's time shift in order to remove the saturation without affecting the contrast.

B. Frequency deviation (percentage frequency change)

Fig. 3 shows the dependence between the contrast and frequency deviation – parameter d in (7) and (8).

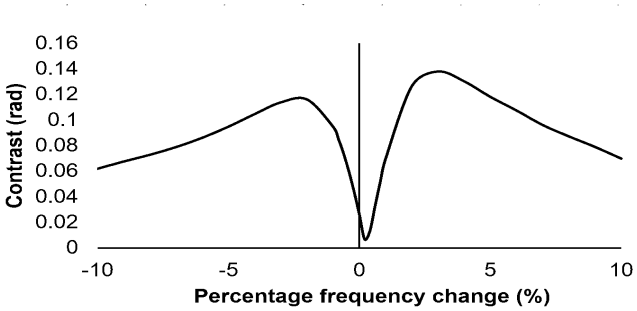

Fig. 3 dependence between contrast and frequency deviation

It can be seen that the change in the correlation function frequency in narrow limits has a great effect on the phase contrast. Consequently, the use of frequency change is useful in cases, where the exact lock-in frequency is not known or its value is unstable over time.

C. Window length and window sliding

In some cases, only temperature signal segment (window) can be processed. The illustrated temperature signal model consists of 500 samples (with 50 samples in one period). Fig. 4 shows the dependence between the phase contrast and window length used in postprocessing. In this case, the window lengths are multiples of the samples number in lock-in period. It should be note that the windows length change can significantly increase or decrease the phase contrast. Postprocessing over all periods can significantly reduce the value of received phase contrast.

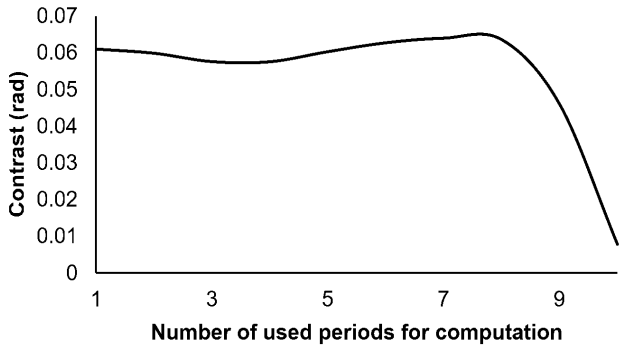

Fig. 4 dependence between phase contrast and number of used periods in post-processing

Fig. 5 shows the dependence between contrast and window sliding offset at window length 350 samples (7 periods) and maximum offset 50 samples (one period).

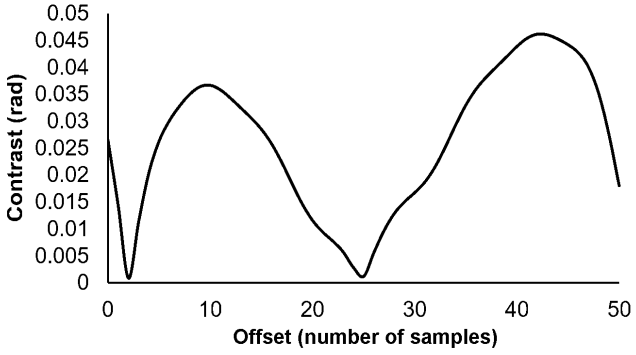

Fig. 5 dependence between phase contrast and window length offset at using 350 samples (respectively thermograms) in processing

It can be seen that the phase contrast tends to zero for some window sliding offset values. Therefore, the choice of the offset is very important for phasegram quality.

Fig. 6 shows the same dependence as in Fig. 5, but the processing is carried out on window length, that is not multiple of the samples number in a lock-in period. There is only one additional sample. The computations are performed on 351 samples instead of 350 samples.

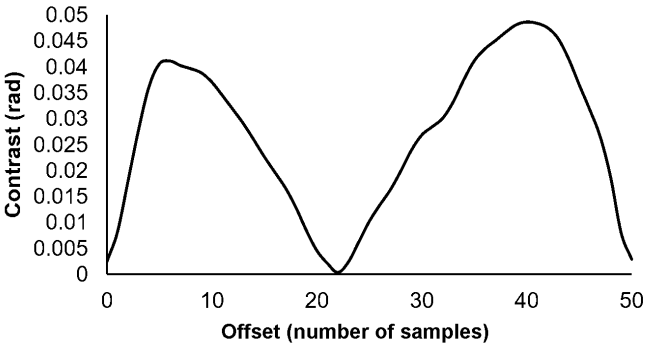

Fig. 6 dependence between phase contrast and offset at using 351 samples (respectively thermograms)

The results from Fig. 6 shows that adding only one additional sample to window can significantly changing the obtained contrast – at Offset = 0 the contrast obtained after processing of window with 350 samples (Fig. 5) is relatively high (0.025), but the contrast after processing of the same window with only one additional sample (Fig. 6) is about ten times lower. Using window sliding approach an approximately the same relatively high contrast can be obtained even when the window length is not multiple of the samples number in a lock-in period (In Fig. 5 and Fig. 6 the maximum obtained contrast is approximately the same – 0.05).

V. Experimental Verification

Real lock-in thermography measurements were performed for verification of the results obtained after the modelling of temperature signals. Two test specimens for the study were prepared.

Photographs of the used test samples are shown in Fig. 7. Glass-reinforced epoxy laminate material (FR4), one-sided laminated with thin layer copper foil was used for the preparation of the test samples.

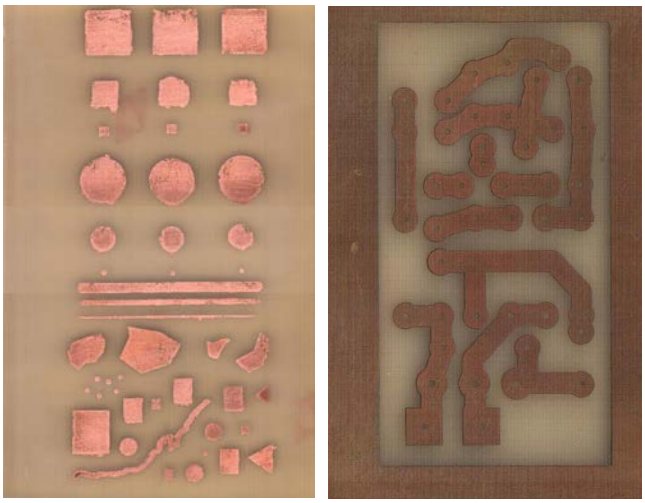

(a) (b)

Fig. 7 test samples used for verification

The test sample, shown in Fig. 7a (test sample A) includes three groups of artificial defects – with large area, with medium area and with small area. In each group, the defects are with approximately equal area, but with different shape (square, circle, triangle, irregular polygon) in order to avoid the influence of the defect shape in the evaluation of the post-processing quality.

The test sample, shown in Fig. 7b (test sample B) includes artificial defects, which are curved lines with high thickness, located very close to each other, i.e. defects whose differentiation is difficult.

The side of the specimens without copper paths is heated with a halogen lamp. The light intensity of the halogen lamp is modulated with a sinusoidal modulation signal. The same side of the test samples is captured with infrared camera (reflection mode lock-in thermography). Measurement parameters are: lock-in frequency - 0.2 Hz (lock-in period – 1 / 0.2 = 5 s); Number of lock-in periods - 10; frame rate of the camera - 10 frames per second (therefore, there are 50 thermograms in one lock-in period – 5 s × 10 frames per second).

The phase calculation is performed using (6), as in the phase calculation of the modelled temperature signals. The same phasegram contrast increasing methods is performed as in the modelled temperature signals post-processing. The phase contrast between defect areas and sound area is used to evaluate the post-processing quality. The phase of each defective area is calculated and resulting phase contrast values for each defect group are averaged. An averaging of 9 pixels for each defective area is performed in order to reduce the impact of the IR detector noise. Fig. 8 shows defective areas and sound area used for contrast computation for test sample A. In Fig.9 are shown defect and sound area used for contrast computation for test sample B.

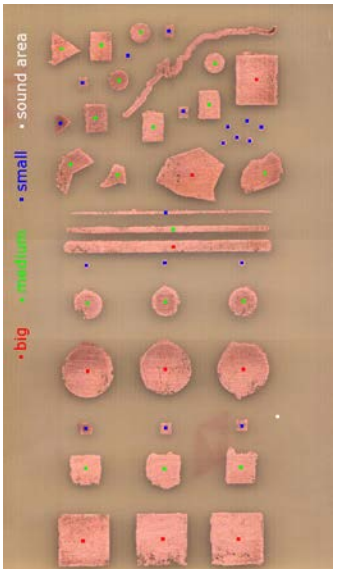

Fig. 8 Defect areas, used for contrast computation for the three groups artificial defects (red, green and blue areas) and sound area (white area)

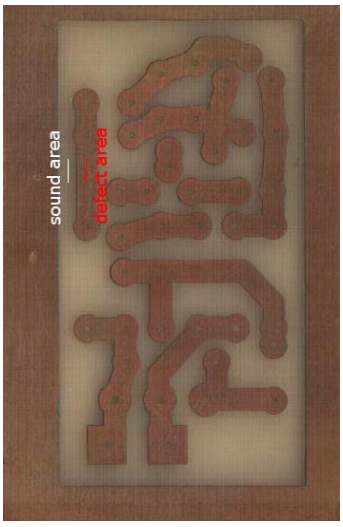

Fig. 9 Defect area (red) and sound area (white), used for contrast computation of the three groups artificial defects (red, green and blue areas) and sound area (white area)

A. Time shift of the correlation function

To confirm the applicability of the method of changing the correlation function's time shift, the method is used in case in which occurs saturation covering partially the region of interest. Fig. 9a shows the phasegram with saturation. It is seen that the phase information of a large number of pixels is lost. Although saturated areas are approaching in shape to defects, the use of the phasegram with saturated pixels for defects evaluation would lead to errors. For example, marked in red areas in phasegram shown in Fig. 10a, where there are no defects, will be perceived as areas with a defect. Phasegram calculations are performed at different time shift values of the correlation function. For some values, significant reduction in saturation areas resulting, even complete phase saturation removal. Fig. 10b shows the phasegram with saturation removed after applying the method.

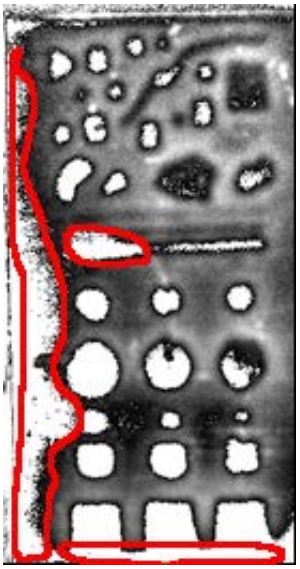
(a)
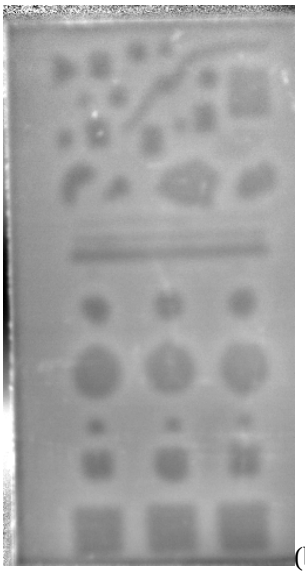
(b)

Fig. 10 Phasegram of test sample A with saturation (a) and after performing time shift changing of the correlation function

B. Selection of window length

The phase contrast for all three groups of defects and the average contrast in test sample A is calculated, when the processing is performed on a different number of periods (from 1 to 10). Dependence is shown in Fig. 11. It can be seen that the effect on the contrast is different for the different groups of defects and calculation for a different number of periods may increase the contrast of the phasegram.

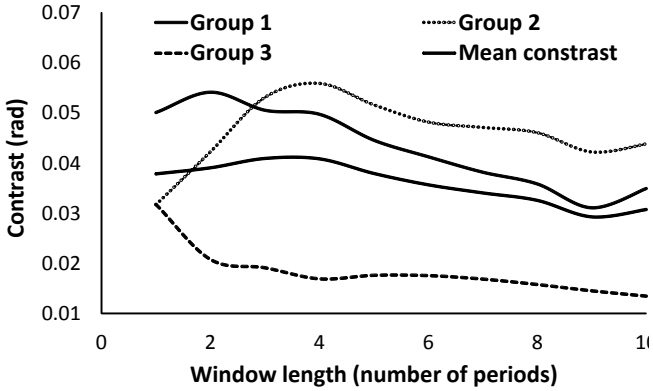

Fig. 11 dependence of phase contrast from window length for test sample A post-processing

C. Performing window sliding approach

Windows sliding approach in the post-processing after lock-in thermography measurement of the two test samples is performed. The phase contrast for the three groups of defects and average contrast for test sample A is calculated. The dependence of the phase contrast from window sliding offset for test sample A is shown in Fig. 12.

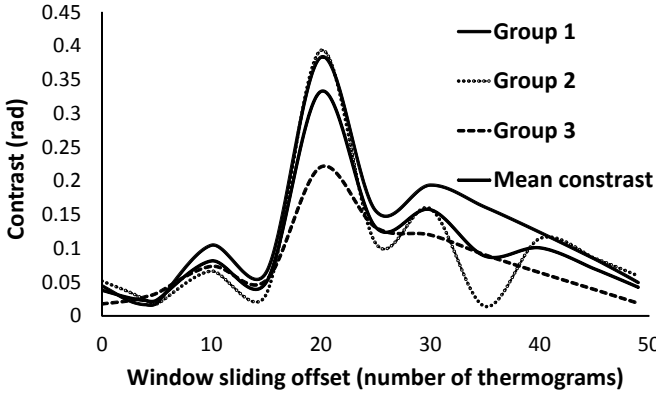

Fig. 12 dependence of phase contrast from used different part of the thermogram sequence (different window sliding offset) for test sample A post-processing

Used thermograms	Contrast (rad)
301-450	0.015952
309-458	0.00079604
328-477	0.12701

Table. III Contrast at different window sliding offset

In Table III is shown results from phase contrast calculation for test sample B at different window sliding offset for sample.

Fig. 13 shows phasegrams of test sample B for values of window sliding offset, shown in Table III.

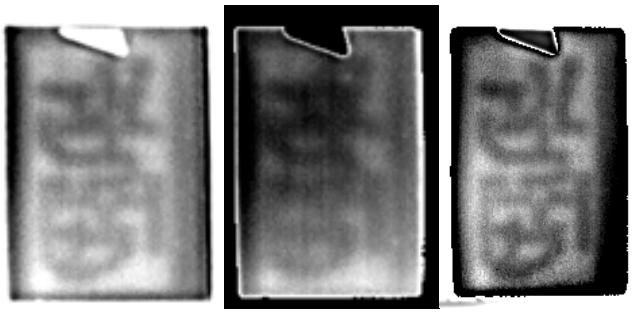

(a) (b) (c)

Fig. 13 phasegram at used different part of thermogram sequence (different window sliding offset) for test sample B (a – 301-450, b – 309-458, c – 328-477)

Fig. 14 shows phasegrams obtained after computation using on window length, that is not multiple of the samples number in a lock-in period. It is performed window sliding offset and the contrast is increased significantly. Fig. 14b shows phasegram with maximum contrast.

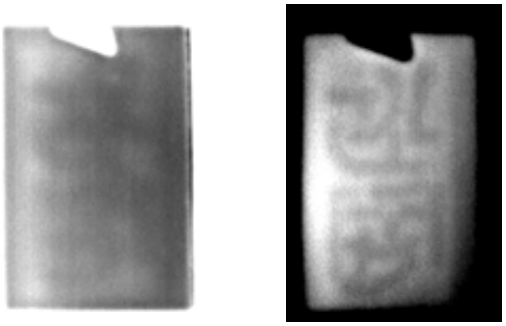

(a) (b)

Fig. 14 phasegram obtained after computation using on window length, that is not multiple of the samples number in a lock-in period for test sample B (a – 300-450, b – 332-482)

Received result confirms the dependence shown in Fig. 6.

The results shown in Fig. 12 and Fig. 13 show that the choice of initial and final thermogram has a significant influence on the contrast. The difference in contrast between Fig. 13b and Fig. 13c is more than one hundred times.

The results shown in Fig. 14 show that when there is a discrepancy between the correlation function and the window length, almost zero contrast can be obtained in some cases, but using a window sliding approach, a phasegram with sufficient contrast to detect the defects may be obtained again.

D. Selection of frequency deviation

The dependence of phase contrast from correlation function's frequency deviation – parameter *d* in (7) and (8) for test sample A is studied. Fig. 15 shows dependence between phase contrast for three groups artificial defects and frequency deviation.

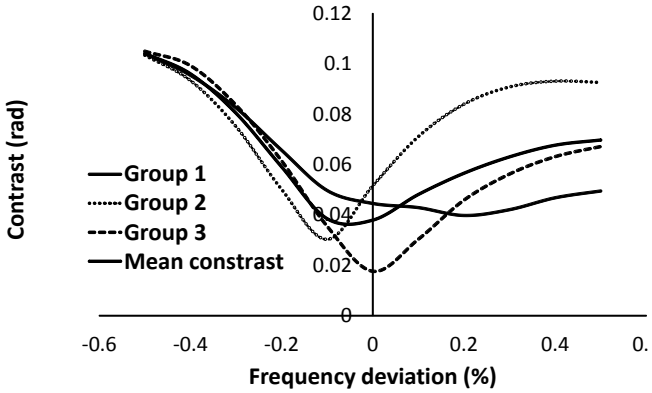

Fig. 15 dependence of phase contrast from frequency deviation for test sample A post-processing

Received results shows that using of frequency deviation changing method can also increase the phase contrast.

E. Problem with sharpness of phasegrams

The methods used to increase phase contrast affect not only the phase contrast, but also the sharpness of the resulting phasegrams (associated with the ability to determine the defects contours and dimensions). Fig. 16 shows phasegrams obtained after the application of the described methods for contrast increasing.

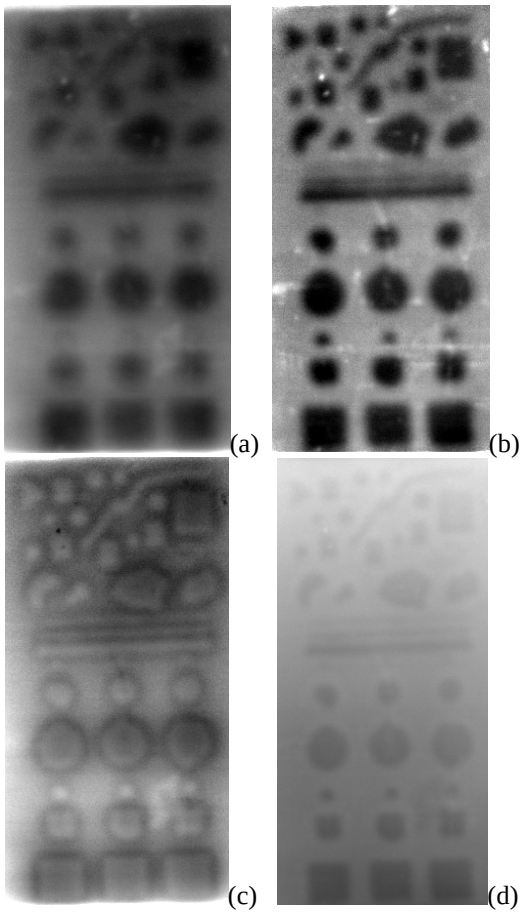

Fig. 16 Examples for phasegrams with good contrast, but with different sharpness

The contrast in all phasegrams shown in Fig. 16 is sufficient to detect the presence of defects. However, sharpness is very different. The phasegram shown in Fig. 16a has a high contrast, but the contours of the defects are highly "blurred". In this case, determining the contours and dimensions of defects is difficult. Even it is difficult to distinguish some defects from one another. In the phasegrams shown in Fig. 16b and Fig. 16c, defects can be clearly distinguished from one another, but their contours and dimensions are also difficult to determine. The phasegram shown in Fig. 16d has smaller contrast than the others shown, but the sharpness is high and the determination of contours and dimensions of the defects will be the more accurate than in other three presented phasegrams.

This problem is related to the different lateral distribution of heat around the defects during the thermography measurement.

Consequently, the proposed methods for contrast increasing are useful in order to avoid cases, where incorrect calculation of the phase leads to very low or even zero contrast between the areas (e.g. Fig. 13b) whose temperature signals have sufficient phase difference. However, the sharpness of the image should also be taken into account when using the contrast increasing methods. Otherwise, phasegrams with high contrast between the defect and sound areas can be obtained, but with "blurred" contours of the defects, which can lead to erroneous determination of the defects' contours and dimensions, and may even make it difficult to distinguish the defects from one another.

VI. Algorithm for Improving Post-Processing Quality

An algorithm for obtaining the maximum quality of the phasegram (a compromise between sufficient contrast and exact determination of the defects' contours and dimensions) is defined based on the obtained results from this study.

Based on results from this study, the contrast of the phasegram depends from:

- the selected window sliding offset;
- the selected window length;
- the frequency of the correlation function.

A block diagram of the algorithm is shown in Fig. 17. The first step of the algorithm is to define defect areas and sound areas. The phase is calculated only for the pixels used to calculate the contrast in order to increase the algorithm performance. The contrast-increasing methods described in this paper is performed – window sliding offset changing, window length changing, frequency deviation changing. If saturation occurs, the corresponding phase calculation is repeated at different time shift of the correlation function until a saturation disappears (the saturated pixel of the phasegram has a value close to 1.57 or -1.57). For the cases, where the contrast is sufficient to detect the searched defects, it is necessary to calculate the whole phasegram and evaluate its sharpness. The method for evaluation of the phasegram's sharpness is not subject of this study.

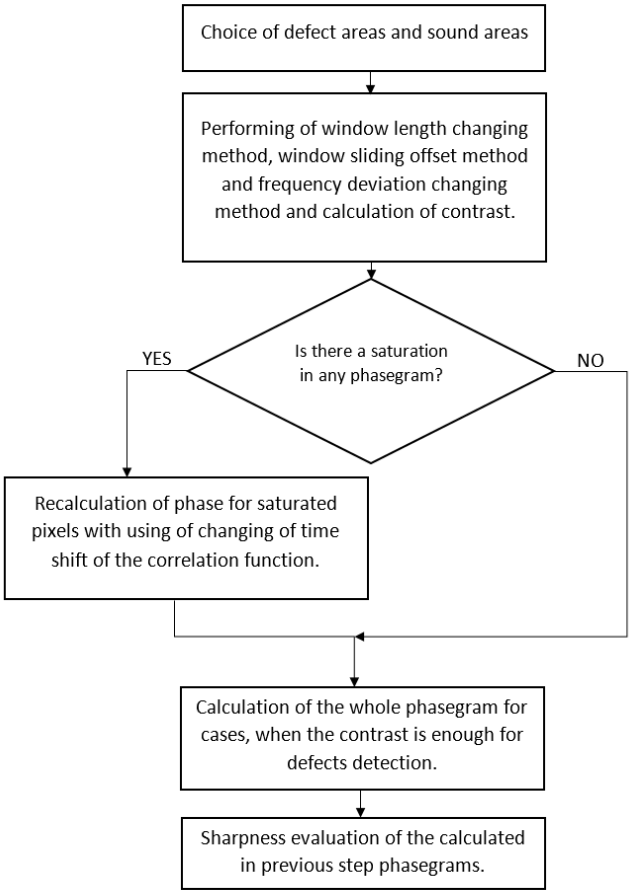

Fig. 17 block algorithm for improving post-processing quality

REFERENCES

[1] M. Vollmer, K.-P. Möllmann, *Infrared Thermal Imaging: Fundamentals, Research and Applications*, Wiley-VCH, 2018.

[2] X. Maldague, *Theory and practice of infrared technology for nondestructive testing*, New York: Wiley, 2001.

[3] O. Breitenstein, W. Warta, M. Langenkamp, *Lock-in Thermography: Basics and Use for Evaluating Electronic Devices and Materials*, New York: Springer, 2010.

[4] G. Pitarresi, "Lock-In Signal Post-Processing Techniques in Infra-Red Thermography for Materials Structural Evaluation", *Experimental Mechanics*, vol. 55, no. 4, pp. 667-680, Apr. 2015.

[5] C. Antolis, N. Rajic, "Optical Lock-in Thermography for Structural Health Monitoring – A Study into Infrared Detector Performance", *Procedia Engineering*, vol. 188, pp. 471-478, 2017.

[6] L. Junyan, T. Qingju, L. Xun, W. Yang, "Research on the quantitative analysis of subsurface defects for non-destructive testing by lock-in thermography", *NDT & E International*, vol. 45, no. 1, pp. 104-110, 2012.

[7] G. Kim, G.-H. Kim, J. Park, D.-Y. Kim, B.-K. Cho, "Application of infrared lock-in thermography for the quantitative evaluation of bruises on pears", *Infrared Physics & Technology*, vol. 63, pp. 133-139, 2014.

[8] H. Zhao, Z. Zhou, J. Fan, G. Li, G. Sun, "Application of lock-in thermography for the inspection of disbonds in titanium alloy honeycomb sandwich structure", *Infrared Physics & Technology*, vol. 81, pp. 69-78, 2017.

[9] A. V. Stoynova, B. B. Bonev, "Specificity in the Optical Excitation Lock-in Thermography Results Processing", *MATEC Web of conferences*, vol. 125, article number 05016, Oct. 2017.

[10] A. V. Stoynova, B. B. Bonev, "Improvement the temperature signal filtering in lock-in thermography", *MATEC Web of conferences*, vol. 210, article number 05007, Oct. 2018.